ARTICLE

Lipid–Quantum Dot Bilayer Vesicles Enhance Tumor Cell Uptake and Retention *in Vitro* and *in Vivo*

Wafa' T. Al-Jamal,[†] Khuloud T. Al-Jamal,[†] Bowen Tian,[†] Lara Lacerda,[†] Paul H. Bomans,[‡] Peter M. Frederik,[‡] and Kostas Kostarelos[†,*]

[†]Nanomedicine Lab, Centre for Drug Delivery Research, The School of Pharmacy, University of London, London WC1N 1AX, United Kingdom, and [‡]Electron Microscopy Unit, Department of Pathology, University of Maastricht, Universiteitssingel 50, 6229 ER Maastricht, The Netherlands

ABSTRACT We report the construction of lipid–quantum dot (L–QD) bilayer vesicles by incorporation of the smallest (2 nm core size) commercially available CdSe/ZnS QD within zwitterionic dioleoylphosphatidylcholine and cationic 1,2-dioleoyl-3-trimethylammonium-propane lipid bilayers, self-assembling into small unilamellar vesicles. The incorporation of QD in the acyl environment of the lipid bilayer led to significant enhancement of their optical stability during storage and exposure to UV irradiation compared to that of QD alone in toluene. Moreover, structural characterization of L–QD hybrid bilayer vesicles using cryogenic electron microscopy revealed that the incorporation of QD takes place by hydrophobic self-association within the biomembranes. The L–QD vesicles bound and internalized in human epithelial lung cells (A549), and confocal laser scanning microscopy studies indicated that the L–QD were able to intracellularly traffick inside the cells. Moreover, cationic L–QD vesicles were injected *in vivo* intratumorally, leading to enhanced retention within human cervical carcinoma (C33a) xenografts. The hybrid L–QD bilayer vesicles presented here are thought to constitute a novel delivery system that offers the potential for transport of combinatory therapeutic and diagnostic modalities to cancer cells *in vitro* and *in vivo*.

KEYWORDS: nanomedicine · imaging · theragnostics · cancer therapy · cervical carcinoma · cryo-EM

Semiconducting nanocrystals known as quantum dots (QD) are fluorescent nanoparticles of 1–10 nm diameter,[1–3] which offer distinct spectrofluorometric advantages over traditional fluorescent organic molecules. QD exhibit fluorescence characteristics that are 10–20 times brighter than those of conventional organic dyes, greater photostability, a broad excitation wavelength range, a size-tunable spectrum, and a narrow and symmetric emission spectrum, ranging from 400 to 2000 nm depending on their size and chemical composition. Due to these photophysical characteristics, they are being explored as potential imaging agents primarily in fluorescence-based diagnostic applications.[3,4]

Most QD types are originally prepared in organic solvents;[5] therefore, their hydrophobic shells compromise their water solubility and consequently their compatibility with the biological milieu. In addition, their hydrophobic surface results in an unfavorable toxicity profile, introducing serious limitations in the potential biomedical and clinical applications of QD. Many strategies are being developed to overcome this limitation. The most successful approach has been to functionalize QD with polar moieties and ligands with specific receptor-recognition signals (such as peptides and monoclonal antibodies or their fragments).[1,6–8] However, this surface modification often leads to decreases in QD fluorescence intensity and photostability,[9–11] which for *in vivo* applications requires higher doses of administered QD and therefore increases potential toxicity burden and risk.

Liposomes constitute the most clinically established type of nanoparticle today, with an extensively investigated pharmacological profile for various therapeutic and diagnostic applications.[12] They consist of a lipid bilayer (hydrophobic region) surrounding an aqueous phase (hydrophilic compartment) and can be engineered to carry different drug molecules of polar or apolar character. Moreover, liposomes offer exceptional engineering versatility because their physicochemical characteristics such as lipid vesicle size, lamellarity (number of concentric lipid bilayers), and surface charge can be easily modified with established methodologies. Preformed liposomes of cationic surface character have been electrostatically complexed with functionalized QD to enhance the cellular binding and internalization of QD for *ex vivo* cell labeling.[13,14] However, these studies simply mixed commercially available, liposome-based transfection agents with hydrophilic QD in order to translocate

*Address correspondence to kostas.kostarelos@pharmacy.ac.uk.

Received for review August 17, 2007 and accepted January 21, 2008.

Published online March 25, 2008.
10.1021/nn700176a CCC: $40.75

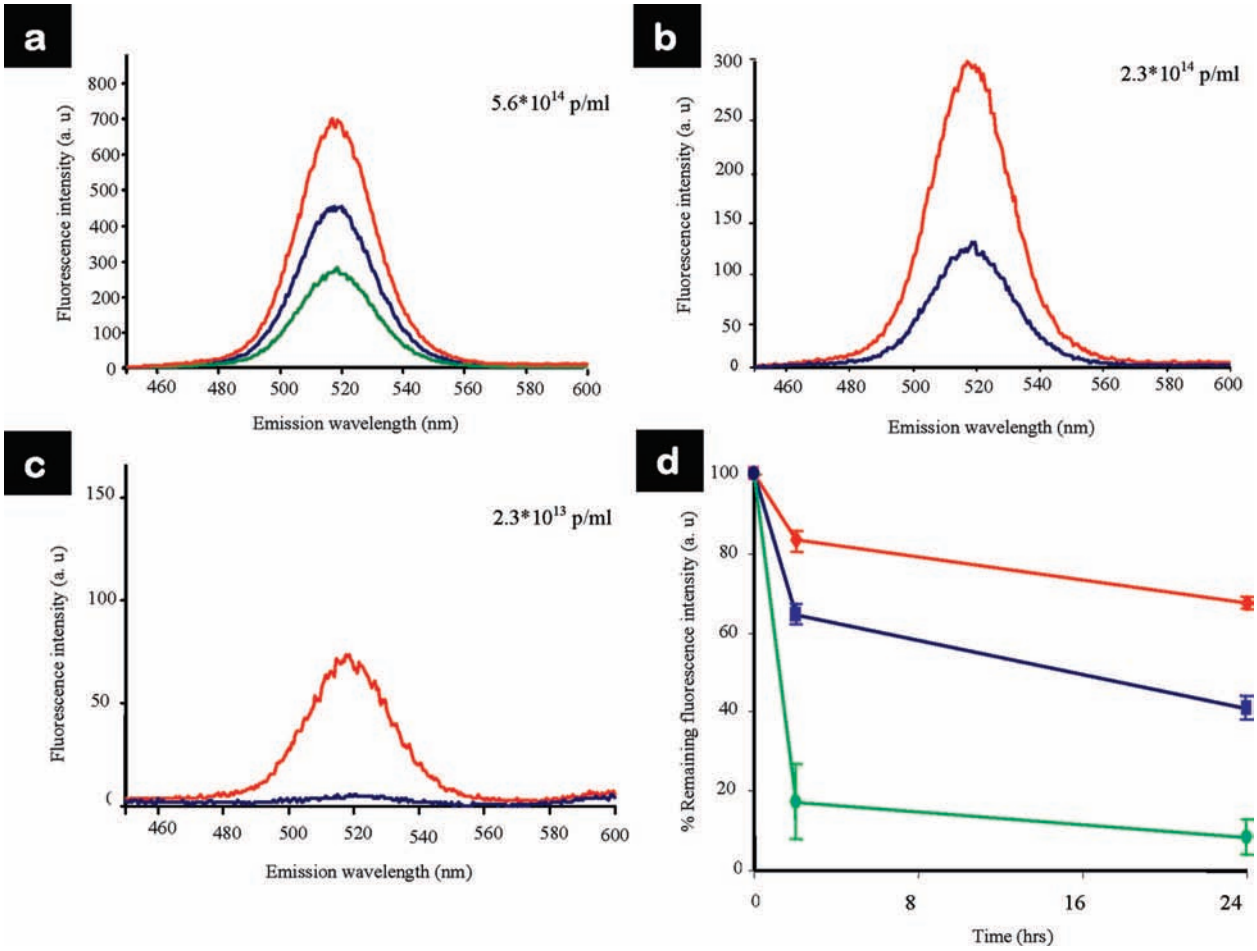

Figure 1. Fluorescence emission spectra (λ_{em} = 517 nm) of different concentrations of CdSe/ZnS core/shell QD immediately after preparation (red), at 24 h (blue), and after 7 days (green) in toluene: (a) 5.6 × 10^{14} p/mL, (b) 2.3 × 10^{14} p/mL, and (c) 2.3 × 10^{13} p/mL. (d) Percentage of remaining QD fluorescence in toluene after 24 h for different QD concentrations: 5.6 × 10^{14} p/mL (red), 2.3 × 10^{14} p/mL (blue), and 2.3 × 10^{13} p/mL (green) (p/mL denotes particles per milliliter).

enough QD particles intracellularly to achieve efficient levels of mammalian cell fluorescent labeling.

In the present work, we report the engineering of hybrid lipid−quantum dot (L−QD) bilayer vesicles by incorporation of organic QD within the vesicle lipid bilayer. Incorporation of QD within liposome membranes retains all the QD fluorescent characteristics and makes hydrophobic QD compatible with aqueous phases, and therefore biological environments. Moreover, we hypothesized that the tight packing of QD within the lipid bilayer will diminish QD shell shedding that commonly leads to photodegradation,[9,15,16] impeding the widespread diagnostic use of QD due to weak fluorescence signals. Furthermore, we studied the ability of the L−QD hybrids to label tumor cells *in vitro* and *in vivo*. Lipid−QD hybrid bilayers were engineered in order to retain the lipid bilayer biocompatibility, lipid vesicle structural, and surface versatility and at the same time preserve the exemplary luminescent characteristics of QD, altogether offering a novel system for potential combinatory therapeutic and diagnostic applications in oncology.

RESULTS

CdSe/ZnS QD Stability in Toluene. The fluorescence intensity of serially diluted CdSe/ZnS QD dispersions in toluene (2 nm core size according to the manufacturer) was monitored over 24 h at 4 °C and in darkness for up to 7 days. As expected, the observed QD fluorescence intensity was found to be concentration-dependent. Higher QD concentrations led to higher fluorescence intensity, as can be seen in Figure 1a−c. Fluorescence intensity decreased in toluene rapidly for dilute QD toluene suspensions, reaching less than 10% of the original intensity within 24 h at a QD concentration of 2.3 × 10^{13} particles (p)/mL (Figure 1d). Fluorescence intensity for the 2.3 × 10^{14} p/mL sample decreased to 50%, and for 5.6 × 10^{14} p/mL QD suspension in toluene, 75–80% of the initial fluorescence intensity was maintained after 24 h (Figure 1d). No change in the fluorescence emission maxima (blue shift) of these samples was detected, which excluded the possibility of QD surface photoxidation.[17,18] No precipitation, aggregation, or other changes in the colloidal properties of the QD toluene dispersions were observed during the storage period of 7 days. These results indicated that QD degra-

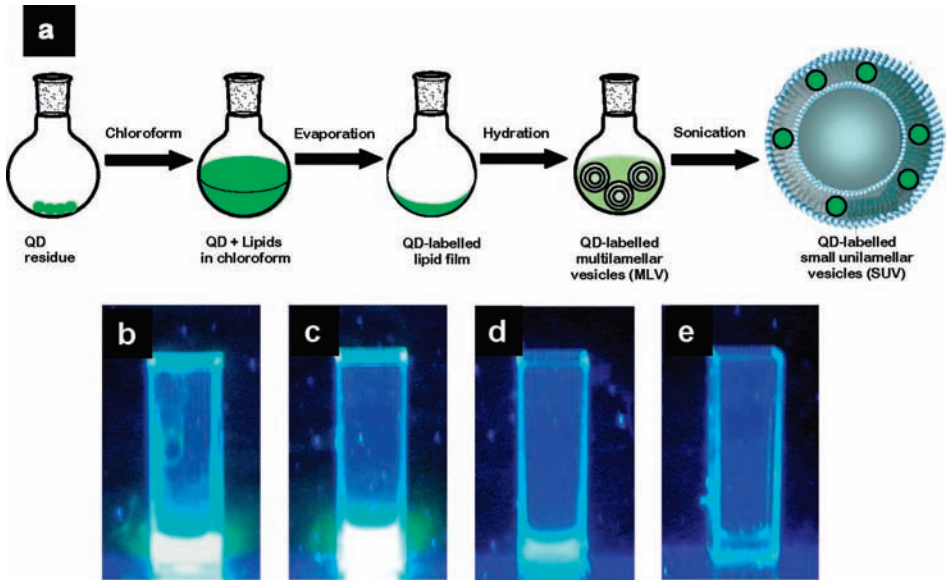

Figure 2. (a) Methodology for the formation of L−QD vesicles. (Bottom) Photographs of (b) 5.6 × 10^{14} p/mL CdSe/ZnS core/shell QD in toluene, (c) L−QD containing 1 mM DOPC suspended in dH_2O, (d) QD in dH_2O (negative control), and (e) DOPC lipid vesicles alone in dH_2O. All photographs were captured by placing the samples, immediately upon preparation, under a UV lamp (312 nm) (Vilber Lourmat, France).

dation in toluene occurred at low concentrations, as described previously.[9]

Incorporation of QD into Lipid Bilayers. In order to preserve the high fluorescence intensity of QD and obtain aqueous solubility of the hydrophobic QD used in this study, 5.6 × 10^{14}p/mL CdSe/ZnS QD were mixed with lipid molecules (dioleoylphosphatidylcholine, DOPC) in chloroform, and vesicles were formed following the lipid film hydration methodology. After evaporation of the solvent in a rotary evaporator, a thin QD-containing lipid film was formed, effluxed with a stream of N_2, and kept until further use. Upon hydration of the L−QD film, multilamellar vesicles (MLV) self-assembled, incorporating the QD into their lipid bilayers. Sonication using an ultrasonic bath led to formation of QD-containing small unilamellar vesicles (SUV). Figure 2a depicts the simple, stepwise methodology followed in this study for the formation of L−QD hybrid bilayer vesicles.

In order to confirm that QD fluorescence is preserved after incorporation into the lipid bilayer environment and that the L−QD bilayers were fluorescent, samples were placed under a UV lamp (312 nm wavelength) immediately upon formation. Figure 2b,c shows that QD in toluene and L−QD in dH_2O exhibited strong fluorescent signals, whereas green QD in dH_2O (negative control) emitted almost no fluorescence (Figure 2d), similar to unlabeled lipid vesicles (Figure 2e).

Fluorescence Properties of L−QD Hybrid Vesicles. The qualitative observations from Figure 2 were further studied quantitatively by fluorescence spectrophotometry. As can be seen from Figure 3, at 350 nm excitation wavelength, the spectral characteristics of QD in MLV (Figure 3b) and SUV (Figure 3c) were not affected compared to those obtained for QD in toluene (Figure 3a). Interestingly, incorporation of QD within the lipid bilayer to form L−QD hybrid vesicles led to enhanced photostability of these systems compared to that of QD (of the same concentration) in toluene. Only 30–40% reduction of the initial fluorescence intensity was observed when the QD were embedded within the MLV and SUV lipid bilayers (Figures 3b,c, red curve), compared to more than 70% loss of fluorescence intensity in the case of QD in toluene suspensions (Figure 3a, red curve). Furthermore, the effect of UV radiation was studied by intermittent exposure of QD in toluene and L−QD to a UV light source (λ_{exc} = 312 nm, Vilber Lourmat, France) 3, 7, and 14 days after preparation. QD in toluene were photochemically unstable when exposed to UV light, witnessed as a sharp reduction in fluorescence intensity and a marked blue shift from 517 to 507 nm (Figure 3d, green curve) at 7 days. Complete loss of fluorescence was obtained for QD in toluene after 14 days of UV exposure (Figure 3d, orange curve). On the other hand, the L−QD exhibited improved photostability after both 7 and 14 days of UV exposure (Figure 3e, green and orange curves). These results indicated that the L−QD improved the photostability of QD on storage and against UV light exposure, which can be attributed to the tight packing of the QD within the lipid bilayer, leading to minimization of trioctylphosphine oxide (TOPO) shell shedding and oxygen accessibility to the QD surface.[9,15–18]

Structural Characteristics of L−QD Hybrid Vesicles. Figure 4 depicts cryogenic electron microscopy (cryo-EM) images of aqueous dispersions of L−QD, using DOPC as the lipid component of the hybrid bilayer. L−QD vesicles with 1,2-dioleoyl-3-trimethylammonium-propane (DOTAP, see Supplementary Figure 3d) and DOPC were well formed, as confirmed by cryo-EM images and verified by transmission electron microscopy (TEM, data not shown), indicating the predominance of SUV (for higher resoultion images, see Supplementary Figure 3). Two different concentrations of DOPC lipid molecules were allowed to self-assemble into vesicles in the absence and in the presence of QD. At low lipid:QD ratios (approximately 1000 phospholipid molecules per QD), some degree of deformation of the vesicle structures was observed, resulting in elongated and deformed vesicular structures (white arrows in Fig-

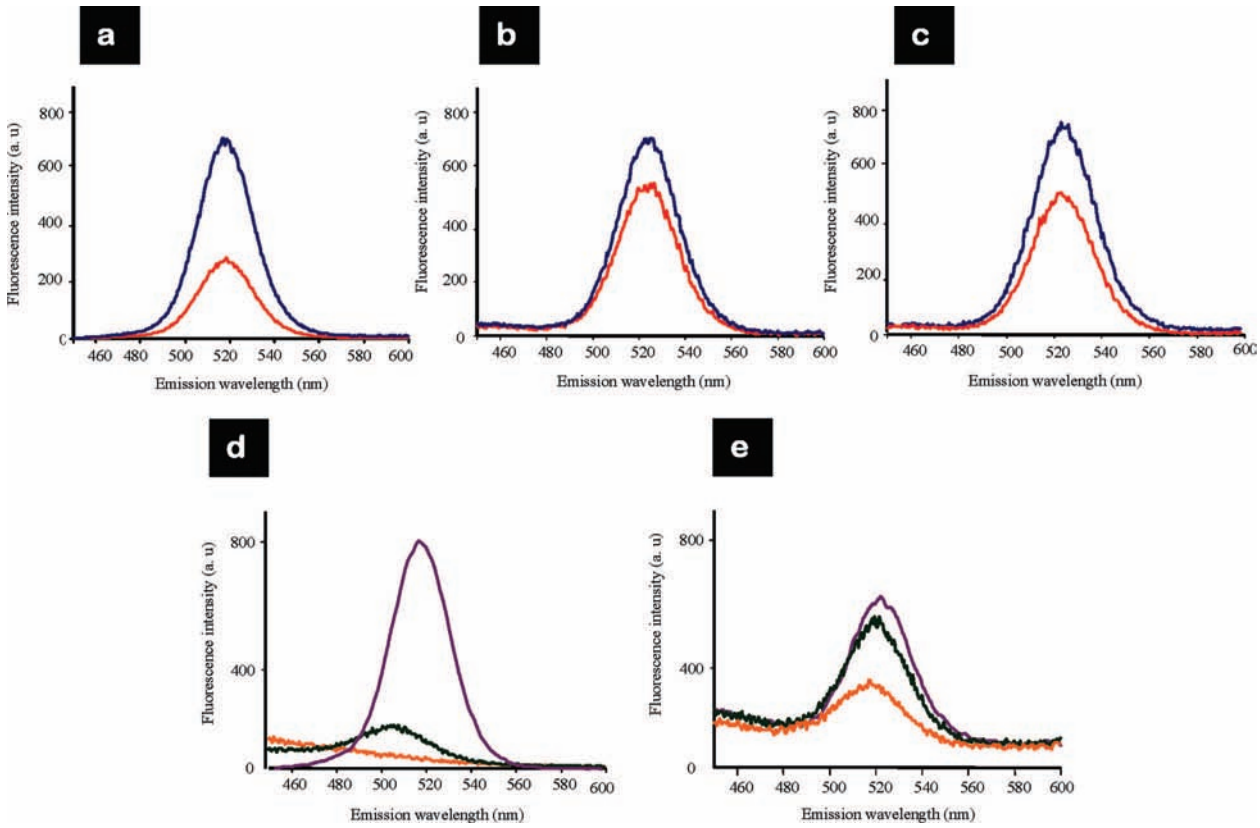

Figure 3. (Top) Fluorescence emission spectra of 5.6 × 10^{14} p/mL CdSe/ZnS core/shell QD immediately after preparation (blue) and after 7 days (red) of storage in (a) toluene (λ_{em} = 517 nm), (b) 1 mM DOPC MLV (λ_{em} = 524 nm), and (c) 1 mM DOPC SUV (λ_{em} = 524 nm). (Bottom) Fluorescence emission spectra of 5.6 × 10^{14} p/mL CdSe/ZnS core/shell QD 3 days (purple), 7 days (green), and 14 days (orange) after preparation and UV exposure (λ_{exc} = 312 nm) (d) stored in toluene and (e) as L−QD (1 mM DOPC) in dH_2O.

ure 4c). Moreover, at specific locations, increased lipid bilayer thickness was observed, similar to a protrusion, which was thought to indicate that incorporation of the QD was taking place in "pockets" rather than being evenly distributed throughout the bilayer (Figure 4c). As the lipid:QD ratio was increased (to approximately 10 000 phospholipid molecules per QD), the structure of the L−QD vesicles resembled more that of liposomes alone, with perfectly spherical vesicles being formed (Figure 4d−f). Interestingly, joined vesicles, connected by a shared region of their bilayer, were observed throughout the L−QD samples (see black arrows in Figures 4d,e). Higher resolution images of such paired vesicles indicated that these regions connecting the vesicles may be bilayer regions shared between vesicles containing the incorporated hydrophobic QD (Figure 4f).

The hydrophobic CdSe/ZnS QD were then successfully incorporated in two types of lipid bilayer vesicles having different surface and bilayer characteristics, the zwitterionic DOPC and the cationic DOTAP liposomes (approximately 1000 phospholipid molecules per QD). The structural characteristics of these L−QD were further studied by dynamic light scattering (Table 1). The mean L−QD vesicle diameter and surface charge were in the range of that obtained for lipid vesicles consisting of the equivalent lipids alone. However, further studies will be required (such as neutron scattering of the L−QD bilayers) to elucidate those structures at the molecular level. All L−QD that have been constructed in our laboratory have consistently produced a mean diameter between 100 and 160 nm (polydispersity index between 0.3 and 0.4). Moreover, these physicochemical characteristics did not change for more than 7 days of storage after preparation, indicating structural and colloidal stability.

Binding and Internalization of L−QD Hybrid Vesicles in Tumor Cells *in Vitro*. In order to study the compatibility and interaction of the novel L−QD hybrid vesicles with the biological milieu, the L−QD were incubated at 37 °C with live mammalian cell cultures. Figure 5a,b depicts confo-

TABLE 1. Size and Surface Charge Characteristics of Lipid Vesicles and L−QD Hybrid Vesicles: Mean Diameter, Polydispersity Index, and Surface Charge of Zwitterionic (DOPC) L−QD and Cationic (DOTAP) L−QD As Obtained Using the Nanosizer ZS

nanoparticle type	mean diameter (nm)[a]	polydispersity index[a]	surface charge (mV)[a]
DOPC liposomes	102 ± 1.06	0.379 ± 0.001	−8.9 ± 1.13
L−QD (DOPC)	91.3 ± 6.90	0.369 ± 0.053	−9.52 ± 1.55
DOTAP liposomes	104 ± 0.19	0.265 ± 0.011	+61.7 ± 4.84
L−QD (DOTAP)	115 ± 2.91	0.312 ± 0.053	+59.8 ± 0.16

[a]Mean ± standard deviation; n = 3.

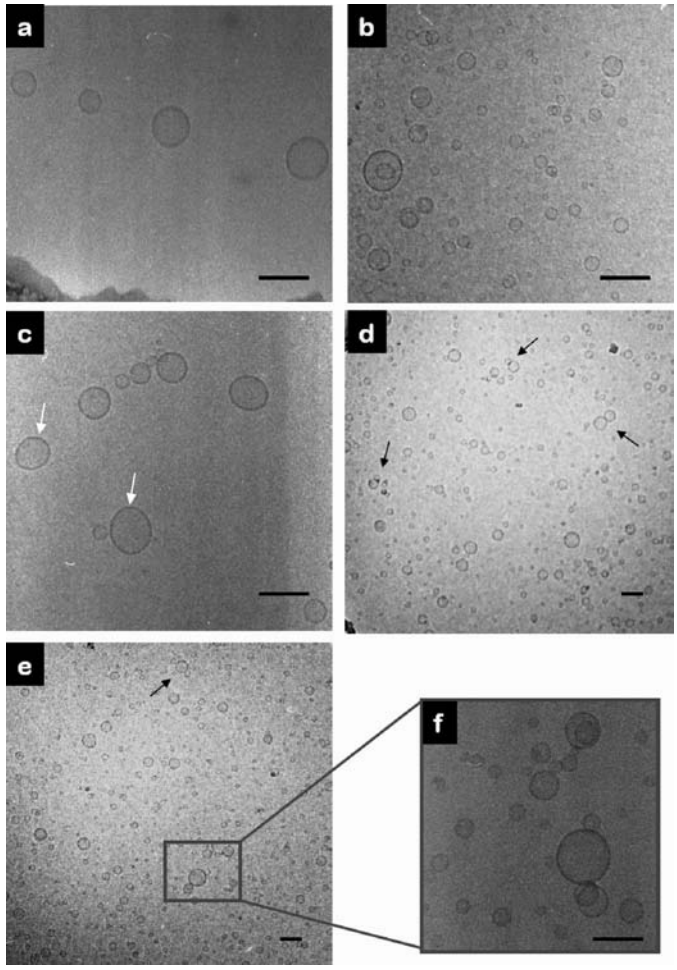

Figure 4. Cryo-transmission electron microscopy images of lipid vesicles at (a) 1 mM and (b) 10 mM DOPC and L−QD hybrid vesicles at (c) 1 mM and (d−f) 10 mM DOPC. Scale bars are 100 nm.

cal laser scanning microscopy (CLSM) images of L−QD vesicles using DOTAP and DOPC lipids, respectively. Both types of L−QD exhibited an intense fluorescent signal in the green channel from the CdSe/ZnS QD present in the lipid bilayer. Human lung epithelial carcinoma A549 cells were cultured, and the L−QD vesicles were added to cells for a 60 min incubation period. The L−QD were bound and internalized within A549 cells, as shown in the CLSM images (Figure 5c−f). Figure 5c−e shows the intracellular uptake for increasing concentrations (0.05–0.2 mM) of the cationic (DOTAP) L−QD vesicles. The L−QD intracellular signal was found to be concentration-dependent for both L−QD types. It is also evident from the CLSM images obtained that L−QD are capable of intracellular trafficking, presumably through endosomal compartments, as they could be imaged throughout the cell volume and close to the nucleus. However, more systematic work needs to be carried out to reveal the exact intracellular trafficking mechanisms for L−QD in comparison to liposomes and QD alone. As expected, the binding and uptake of cationic L−QD (Figure 5e) was much more effective compared to that of DOPC-containing L−QD of neutral surface charge (Figure 5f). These data indicated that L−QD hybrid vesicles were compatible with live cells, capable of cellular uptake and intracellular trafficking.

Uptake and Retention of L−QD Hybrid Vesicles in Tumor Xenografts *in Vivo*. The results from the cell internalization studies *in vitro* led us to investigate how L−QD vesicles would interact with tumor cells in living animals. The L−QD bilayers were engineered with added features to make them more suitable for *in vivo* studies. Cholesterol was incorporated into the lipid bilayer during L−QD hybrid formation to enhance the liposome stability *in vivo*,[19,20] and the fusogenic lipid DOPE was also incorporated to increase L−QD vesicle diffusion within the tumor mass, as previously described for lipid vesicles.[21] Human cervical carcinoma (C33a) xenografts were implanted subcutaneously and grown in CD-1 nude mice. Two different L−QD types were compared, the cationic DOTAP:DOPE:Chol (2:1:1.5) and the zwitterionic DOPC:Chol (2:1), both approximately 100 nm in average diameter and having surface charges of +47.5 and −4.5 mV, respectively. The L−QD were injected intratumorally into fully grown C33a tumor xenografts with a dose of 400 nmol of lipid containing 48 pmol of QD. Mice were killed 5 min or 24 h after injection, and tumors were snap-frozen, cryo-sectioned, fixed, and imaged. The cell nuclei were counterstained with propidium iodide (PI) to evaluate the L−QD localization, retention, and distribution within the tumor volume.

Almost no fluorescent signal was detected in tumor sections injected with the zwitterionic L−QD (DOPC:Chol) vesicles as early as 5 min post-injection (Figure 6b). In contrast, high-intensity green fluorescent signals were obtained from all sections of the tumors injected with cationic L−QD (DOTAP:DOPE:Chol), after both 5 min and 24 h (Figure 6c,d). After 5 min, the cationic L−QD were mainly localized into the interstitial space of the tumor or bound onto the tumor cell membranes (Figure 6c). At 24 h post-administration, the L−QD vesicles were uptaken by tumor cells and had translocated closer to the nucleus (Figure 6d).

DISCUSSION

Semiconducting nanocrystals are developed as optical probes for a variety of biomedical applications.[22,23] The optical and colloidal stability of QD in aqueous environments is essential to allow development of QD-based, clinically relevant diagnostics. The present study showed that commercially available TOPO-capped CdSe/ZnS QD were optically unstable when stored in toluene kept in the dark or under UV light exposure. Similar observations have been previously reported by Kalyuzhny *et al.* and Bullen *et al.* using TOPO-capped CdSe QD dispersed in chloroform (QD concentration between 10^{-7} and 10^{-6} M)[9,15] and in toluene (QD concentration 2 μM).[15] The optical instability of QD is thought to occur due to desorption of the hydropho-

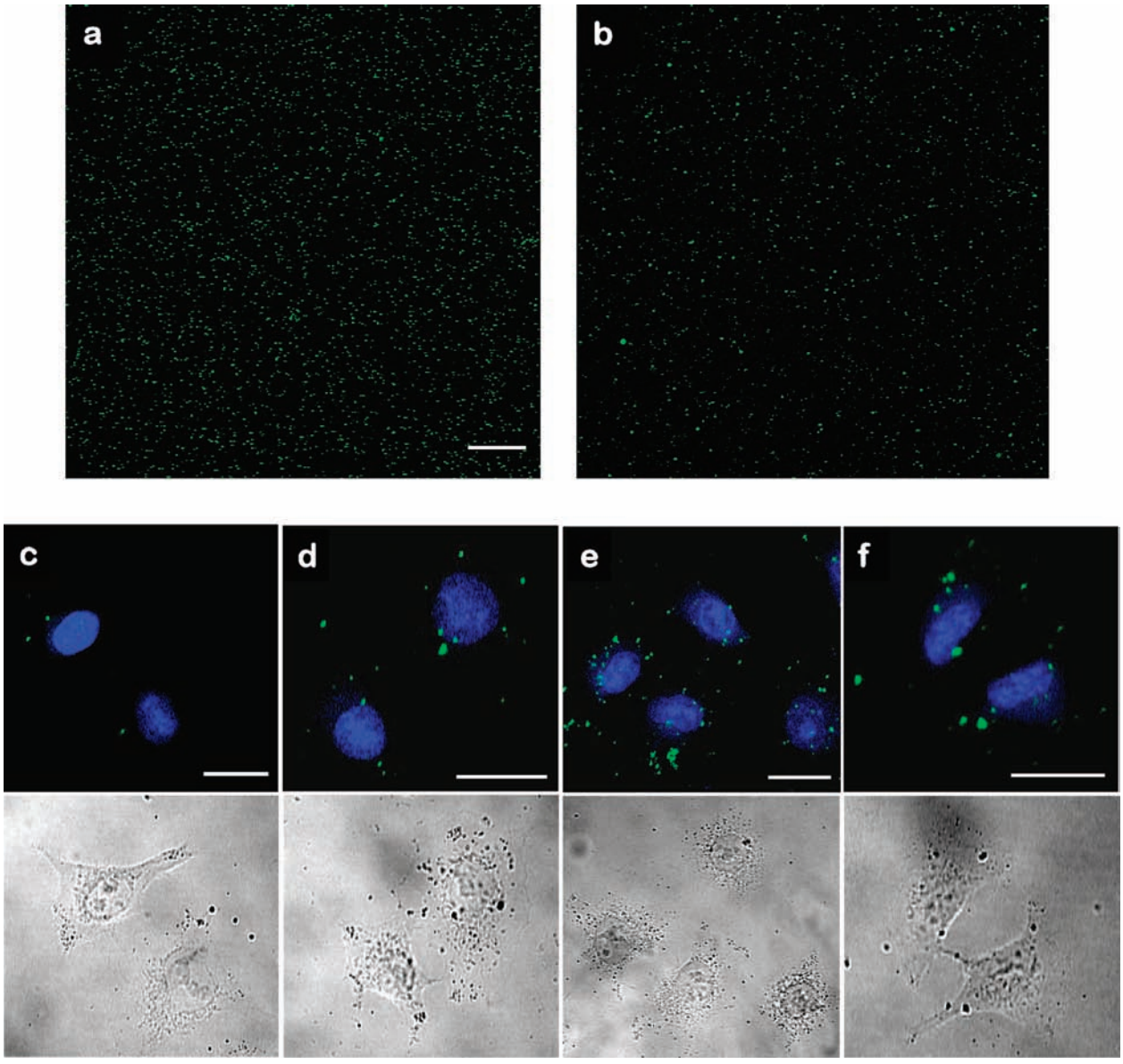

Figure 5. (Top) CLSM images of L−QD with (a) DOTAP and (b) DOPC lipids. (Bottom) Confocal and DIC images of A549 cells after 60 min incubation with different concentrations of cationic (DOTAP) L−QD at (c) 0.05 mM, (d) 0.1 mM, and (e) 0.2 mM and (f) L−QD at 0.2 mM DOPC. Cell nuclei were counterstained with TO-PRO 3. Scale bars are 20 μm.

bic TOPO ligand from the QD surface.[9,15,16] TOPO desorption is dependent on the degree of its solubility to the organic solvents, with higher QD optical stability reported in octane than in toluene.[16] Moreover, TOPO desorption also affects the colloidal stability of QD dispersions,[9] leading to instability.

Attempts to modify the nanocrystal surface to achieve greater aqueous solubility by substitution of the TOPO organic ligand with hydrophilic moieties resulted in changes in the QD absorption and emission spectra and their chemical stability.[9–11] Alternative methodologies that have preserved QD optical properties include coating QD with amphiphilic polymers[6,7,24,25] and phospholipid micelles.[26–29] Very recently, lipid bilayer incorporation of hydrophobic QD has been described independently by others.[30] The present study, carried out almost simultaneously with the studies by Gopalakrishnan *et al.*, is in complete agreement that construction of L−QD bilayer vesicles by incorporation of hydrophobic QD within the lipid bilayer of unilamellar vesicles is possible, further extending the utilization of such hybrid systems to an *in vivo* setup. Moreover, the present study illustrates that incorporation of QD in the acyl environment of the bilayer leads to significant enhancement of their optical stability during storage compared to that of QD in toluene. This enhanced stability can be attributed to minimization of the QD photoxidation and TOPO desorption from the nanocrystal surface. Other studies have reported mixing of water-soluble, functionalized QD with preformed liposomes to enhance plasma membrane translocation. Derfus *et al.* and Hsieh *et al.* showed the high labeling efficiency of water-soluble QD

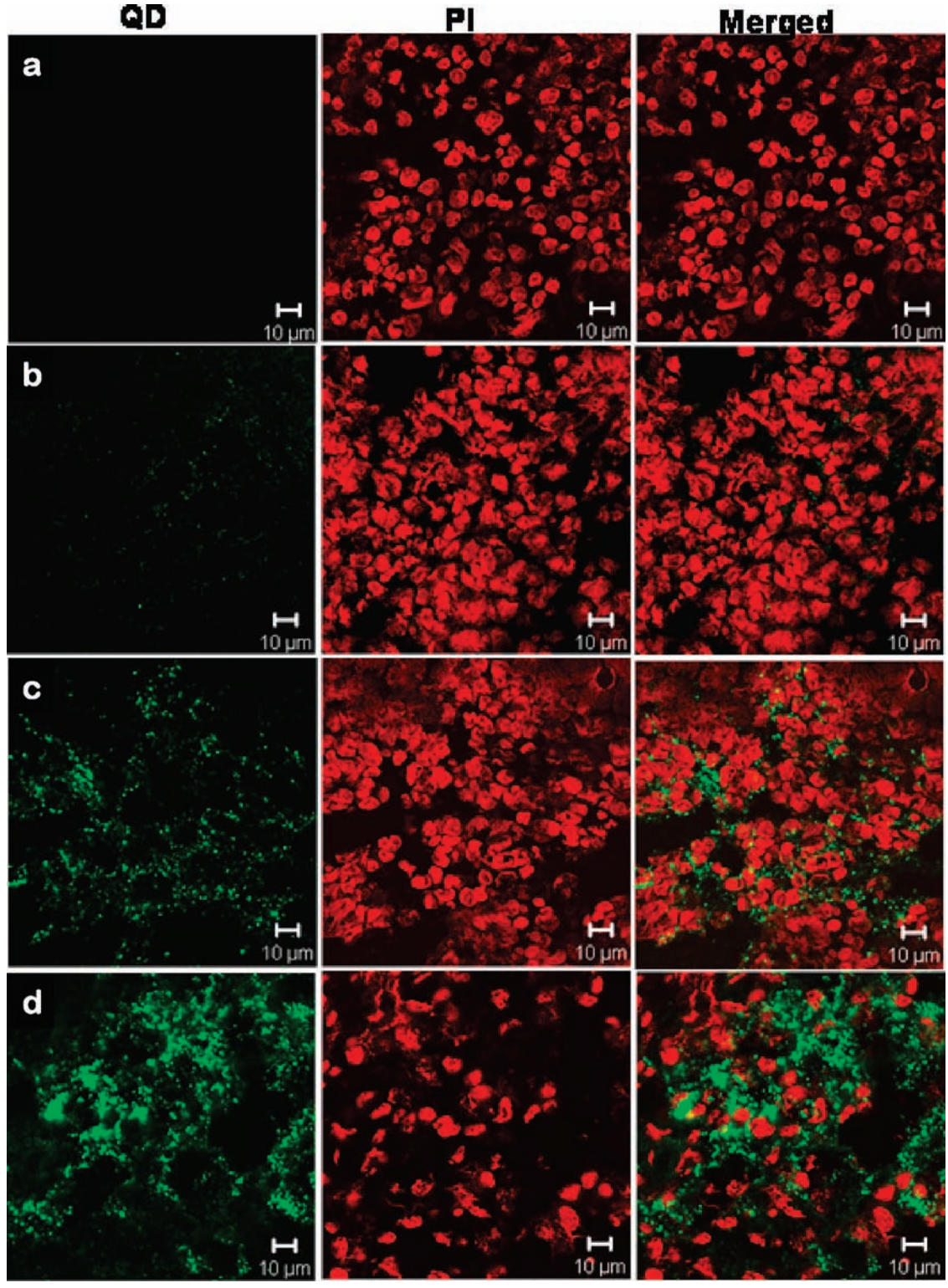

Figure 6. ***In vivo*** **tumor xenograft uptake and retention of L−QD hybrid vesicles. CLSM images of human cerivcal carcinoma (C33a) tumors dissected 5 min after intratumoral injection with (a) 5% dextrose, (b) zwitterionic L−QD (DOPC:Chol; 2:1), and (c) cationic L−QD (DOTAP:DOPE:Chol; 2:1:1.5), and (d) 24 h post-injection of cationic L−QD hybrids. Left panels, L−QD fluorescence; middle panels, PI-stained nuclei; and right panels, the merged green and red channels. Scale bars are 10 μm.**

complexed with lipofectamine (commercially available cationic liposome-based reagent) compared to other carriers;[13,31–33] however, those studies did not attempt the construction of L−QD bilayer vesicles. In the present, study structural characterization by cryo-EM of the L−QD hybrid vesicles revealed that unilamellar vesicles are formed by incorporation of the hydrophobic QD in their lipid bilayer. Interestingly, QD incorporation was evidenced as electron-dense (high contrast, dark) pockets or overall darker bilayers (Figure 4 and Supplementary

Figure 3) but was not identical for all vesicles in the sample.

Quantum dots have been successfully used as fluorescent tags of implanted cells for *in vitro* and *in vivo* imaging of different cell types without affecting cell viability and function.[3,28,34] More recently, functionalized QD have been explored as markers of intracellular compartments[35] or sensors of intracellularly localized molecules.[36,37] Many techniques have been employed to achieve efficient QD cell labeling, such as microinjection, electroporation, and liposome transfection.[13,14,31] Electroporation is a robust technique; however, it is inconvenient for labeling large numbers of cells and generally leads to a high percentage of cell death. Also, the application of an electrical field has been found to induce QD aggregation (500 nm).[13] Although microinjection has been shown to be superior to electroporation for individual cell labeling by QD, each cell needs to be manipulated separately.[13,27] It has been shown that cationic liposomes can bind to the negatively charged plasma membrane, mediate endocytosis, and be used for intracellular delivery of QD,[13,14,31,37,38] but functionalized QD are still required to be complexed with preformed cationic liposomes.

In this work, we report efficient uptake of L−QD hybrid vesicles by cancer cells *in vitro* and, more importantly, retention and uptake by tumor cells *in vivo* by intratumoral administration directly into xenografts. Intratumoral (i.t.) administration offers an alternative way to either label solid tumor cells (to monitor their migratory patterns) or deliver cytotoxic agents locally at the tumor site, and it is clinically relevant for well-localized solid tumors (*e.g.*, head and neck, cerebral carcinomas). However, rapid clearance by the lymphatic drainage system is still the main obstacle for widespread clinical use of such procedures, as has been recently validated by injecting radiolabeled colloids into breast cancer patients to map their sentinel lymph nodes.[39,40] Localization and retention of different anticancer drugs and delivery systems in the tumor mass by i.t. administration has also been extensively studied.[41–45] The clearance rate from the tumor volume is highly dependent on the nanoparticle molecular weight and surface charge. Nomura *et al.* studied the correlation between particle size and surface charge with their retention in tissue-isolated tumors after i.t. injection.[43] They reported that zwitterionic delivery systems (emulsions and liposomes) around 100 nm in diameter were leaking from the tumor immediately after administration. On the other hand, positively charged particles of average size between 100 and 200 nm significantly increased tumor retention from 10−40% to 70–90% after 2 h.[43] Similar results were obtained following i.t. administration of low-molecular-weight mitomycin C conjugated to cationic dextran.[44] Such data are in full agreement with our observations herein, where cationic L−QD vesicles were uptaken by tumor cells in monolayers (Figure 5) and retained within tumor xenografts *in vivo* (Figure 6), in contrast to zwitterionic L−QD vesicles that were drained out of the xenografts within 5 min following i.t. administration. Toward clinical translation of L−QD hybrid vesicles as an imaging modality, the issue of background tissue autofluorescence will be particularly important. The construction of L−QD hybrids using a lead sulfide core, near-infrared-emitting QD with core diameters between 2 and 9 nm, which are now commercially available, can offer great advantages for deep tissue imaging applications.

CONCLUSION

In conclusion, we engineered cationic L−QD hybrid vesicles that electrostatically interacted with the tumor cell membrane *in vitro*, localized, and were retained within the tumor interstitium and tumor cells *in vivo* upon intralesional administration. Such L−QD hybrid vesicles are thought to constitute a facile tool for more efficient labeling of cells using hydrophobic QD without the need of prior QD functionalization to achieve water solubility. Moreover, we envisage that such L−QD hybrid vesicles can be targeted to tumor cells by coupling binding ligands onto the lipid bilayer surface using established lipid-based conjugation chemistry. In this way, QD optical stability and high levels of emitted fluorescent signals will be maintained by minimization of the required injected QD doses to allow effective *in vivo* detection. Furthermore, the vesicular morphology of L−QD hybrids allows loading of their internal aqueous phase with therapeutic molecules (for example, anthracycline molecules such as doxorubicin) toward a potential bimodal (theragnostic) system for the simultaneous delivery of therapeutic and diagnostic agents in malignant tissues.

METHODS

CdSe/ZnS core/shell trioctylphosphine oxide (TOPO)-capped quantum dots (QD) were obtained from Evident Technologies (USA), supplied in toluene with a reported CdSe core size of 2 nm diameter and an overall QD diameter of 4–5 nm, including the 1–2 nm thickness of the organic coat.[7] They exhibited an absorption peak at 502 nm and an emission peak at 517 nm. Red-emitting (600 nm) CdSe/ZnS QD with a core size of 4 nm diameter and an overall size of 6–7 nm diameter were also studied. However, these QD could not be successfully incorporated into the lipid bilayer due to the overall QD size being larger than the lipid bilayer thickness (approximately 4 nm) (see Supplementary Figures 1 and 2). Dioleoylphosphatidylcholine (DOPC, 98%) was obtained from Lipoid GmbH (Germany); 1,2-dioleoyl-3-trimethylammonium-propane (chloride salt) (DOTAP, 99%) from Avanti Polar Lipid (USA); Dulbecco's modified eagle medium (DMEM), fetal bovine serum (FBS), penicillin/streptomycin, and phosphate buffered saline (PBS) from Gibeco (Invitrogen); human epithelial lung cells A549 and human cervical carcinoma C33a from ATCC (USA); TO-PRO 3 in dimethyl sulfoxide solution and propidium iodide (PI) from Molecular Probes (USA); 16-chambered slide from Nunc (USA); RNase A enzyme, Triton X-100, chloroform, and methanol from Sigma (UK); toluene (low in sulfur) from Fisher Scientific (UK); and 1.5–2.5 mm glass beads

from BDH (UK). Deionized water (dH_2O) was used in all preparations.

QD Stability in Toluene. QD stock dispersion in toluene was further diluted to 5.6×10^{14}, 2.3×10^{14}, and 2.3×10^{13} p/mL (p/mL denotes particles per milliliter). The dispersion were flushed with a N_2 stream to reduce the QD oxidation and stored in the dark at 4 °C. The fluorescence intensity was monitored for the freshly prepared dispersion for periods ranging between 1 and 14 days.

Lipid−Quantum Dot Hybrid Vesicle Preparation. DOPC, DOPC:Chol (2:1), DOTAP, and DOTAP: DOPE:Chol (2:1:1.5 molar ratios) were dissolved in chloroform:methanol (4:1 v/v). Multilamellar vesicles (MLV) were prepared by evaporating the organic solvent in a rotary evaporator under vacuum at 40 °C for 30 min and then flushing with a N_2 stream to remove any residual traces of organic solvent. The dried lipid film was hydrated with 1 mL of 0.2 μm filtered dH_2O. The hydrated film was vortexed with 1.5–2.5 mm glass beads for 6 min. Small unilamellar vesicles (SUV) were prepared by further bath sonication (ultrasonic cleaner, VWR) at 30 °C for 5–10 min. The final lipid concentration was 1–10 mM. For L−QD preparation, the organic QD in toluene were incorporated within the lipid bilayer by evaporating 10 μL of QD in toluene under a N_2 stream at room temperature, to avoid the phase separation between toluene and chloroform and to achieve a homogeneous distribution of QD within the lipid film. The green residue was resuspended in the chloroform solution containing the phospholipid, and the process proceeded as above. The final QD concentration in all L−QD preparations was 5.6×10^{14} p/mL. All L−QD samples were flushed with N_2 and stored at 4 °C. The L−QD mean diameter and surface charge were measured by using a Zetasizer Nano ZS instrument (Malvern, UK).

Spectrophotometry and Spectrofluorometry. The QD absorbance spectrum in toluene was collected with a Varian Cary 3E UV−visible spectrophotometer. The scanning rate was 600 nm/min with a 1 cm path length; a 300 μL quartz cuvette was used (Hellma, Scientific Laboratory Supplies Ltd., UK). The emission spectra of CdSe/ZnS core/shell QD in toluene or within lipid bilayers were obtained at a scan rate of 1200 nm/min with a 1 cm path length, in a 300 μL quartz cuvette (Hellma, Scientific Laboratory Supplies Ltd., UK), with excitation and emission slit widths 5 and 10 nm or 10 and 3 nm, respectively, depending on the sample fluorescence, using a Perkin- Elmer LS 50B luminescence spectrometer. All samples were excited using 350 nm wavelength light.

Cryo-Transmission Electron Microscopy. Sample preparation for cryo-transmission electron microscpy (cryo-TEM) was carried out in a temperature- and humidity-controlled chamber using a fully automated (PC-controlled) vitrification robot (Vitrobot, patent applied).[46] A specimen grid was dipped into a suspension and withdrawn, and excess liquid was blotted away. Thin films were formed between the bars of the grids. To vitrify these thin films, the grid was shot into melting ethane. The grids with vitrified thin films were analyzed in a CM-12 transmission microscope (Philips, Eindhoven, The Netherlands) at −170 °C using a Gatan-626 cryo-specimen holder and cryotransfer system (Gatan, Warrendale, PA). The vitrified films were studied at 120 kV and at standard low-dose conditions, and micrographs were taken. Some of the high-resolution cryo-TEM images (Supplementary Figure 3) were obtained using the FEI Life Science TITAN (Eindhoven, The Netherlands), a 300 kV FEG microscope designed for high-contrast imaging. This microscope is equipped with a Gatan 2048 × 2048 CCD camera and a Gatan energy filter.

Interaction of L−QD with Mammalian Cell Cultures. A total of 2×10^4 human epithelial lung cells (A549) were seeded in a 16-chamber slide in DMEM supplemented with 10% FBS and 1% penicillin/streptomycin. Cells were allowed to attach overnight. A 1 mM L−QD solution was diluted by dH_2O further to 0.5 and 0.25 mM. Twenty microliters of each sample was diluted in 80 μL of serum-free DMEM medium and then added to each well. A549 cells were incubated with the L−QD for 60 min at 37 °C and 5% CO_2 and then washed three times with 200 μL of PBS, pH 7.4. The cells were fixed with 150 μL of 2% paraformaldehyde in PBS for 60 min at 4 °C and then washed three times with PBS. A549 cells were perameabilized with 100 μL of 0.1% Triton X-100 in PBS for 10 min at 4 °C and then washed. The nucleus was counterstained with 100 μL of nuclear stain (1 μg/mL TO-PRO 3 and 100 μg/mL RNase A in PBS) for 30 min at 37 °C and then washed. The cells were mounted with citifluor AF1 antifade (Citifluor, UK) and examined under confocal laser scanning microscopy (CLSM).

Animal and Tumor Xenograft Implantation Studies. All animal experiments were performed in compliance with the UK Home Office Code of Practice for the Housing and Care of Animals Used in Scientific Procedures. Six-week-old female CD-1 nude mice (Charles River Laboratories, UK) were caged in groups of five with free access to water. A temperature of 19–22 °C was maintained, with a relative humidity of 45–65%, and a 12 h light/dark cycle. Mice were inoculated with 1×10^7 C33a human cervical carcinoma cells in a volume of 100 μL PBS, subcutaneously into the shaved right flank, using 26G needles. The tumor volume was estimated by measuring three orthogonal diameters (*a*, *b*, and *c*) with calipers; the volume was calculated as $(a \times b \times c) \times 0.5$ mm^3. Intratumoral injections were performed when the tumor reached 62.5 mm^3. For intratumoral administration and tissue analysis, mice were anesthetized using isofluorane and injected with 50 μL of L−QD (equivalent to 400 nmol of lipid and 48 pmol of QD) prepared in 5% dextrose composed of DOPC:Chol (2:1) or DOTAP:DOPE:Chol (2:1:1.5), prepared as described earlier. The needle was inserted in the longitudinal direction from the tumor edge into the center of the tumor, 50 μL of the solution was administered slowly over 1 min, and the needle was left in the tumor for another 5 min to prevent the sample leakage. Either 5 min or 24 h later, the mice were killed, and tumor tissue was harvested and snap-frozen immediately into liquid-nitrogen-cooled isopentane. Samples were stored at −80 °C prior to frozen sectioning. Frozen tumors were embedded into OCT and plunged into a liquid nitrogen bath for at least 30 s. Samples were retrieved from the bath and then sectioned using the cryostat at −18 °C into 5–6 μm thick sections. The sections were mounted on superfrost slides and left to dry at room temperature for 15–30 min. For tumor visualization, the sections were fixed for 3 min in cold acetone at −20 °C, rinsed with PBS for 15 min at room temperature, followed by PI nuclear staining [RNAase treatment (100 μg/mL) for 20 min at 37 °C and incubation with PI solution (1 μg/mL) in PBS for 1–5 min], and then rinsed three times with PBS. Coverslips were mounted with aqueous poly(vinyl alcohol) Citifluor reagent mixed with AF100 antifade reagent (1:10) prior use (Citifluor, UK) and visualized under an X63 oil immersion lens using CLSM.

Confocal Laser Scanning Microscopy. All confocal images were captured with CLSM using a Zeiss LSM 510 Meta instrument. The lasers used were a 30 mW, 488 nm argon laser (for green QD), a 1 mW, 543 nm HeNe laser (for PI), and a 5 mW, 633 nm HeNe laser (for TO-PRO 3). The emission was collected using a band-pass filter between 505 and 530 nm for green QD, a 560 nm long-pass filter for PI, and 649–735 nm for TO-PRO 3.

Acknowledgment. This work was partially supported by The School of Pharmacy, University of London. The authors acknowledge Lipoid Co. (Germany) for the lipid sample gifts and Evident Technologies (New York) for the collaborative agreement on the provision of quantum dots, Ms. Elisabetta Bizzarri for her help in xenograft inoculation, and Mr. Stephen Davison (The Department of Histopathology and Cytopathology, Royal Free Hospital) for tumor cryo-sectioning. W.T.A.-J. is the recipient of the Overseas Research Student Award Scheme (ORSAS) from the University of London. K.T.A.-J. is a recipient of the Maplethorpe Fellowship, The University of London.

Supporting Information Available: Detailed descriptions of L−QD hybrid vesicles containing red-emitting QD nanoparticles, cryo-EM, and confocal images of L−QD hybrids. This material is available free of charge *via* the Internet at http://pubs.acs.org.

REFERENCES AND NOTES

1. Akerman, M. E.; Chan, W. C.; Laakkonen, P.; Bhatia, S. N.; Ruoslahti, E. Nanocrystal Targeting in Vivo. *Proc. Natl. Acad. Sci. U.S.A* **2002**, *99*, 12617–12621.

2. Alivisatos, A. P. Semiconductor Clusters, Nanocrystals, and Quantum Dots. *Science* **1996**, *271*, 933–937.
3. Michalet, X.; Pinaud, F. F.; Bentolila, L. A.; Tsay, J. M.; Doose, S.; Li, J. J.; Sundaresan, G.; Wu, A. M.; Gambhir, S. S.; Weiss, S. Quantum Dots for Live Cells, in Vivo Imaging, and Diagnostics. *Science* **2005**, *307*, 538–544.
4. Parak, W. J.; Pellegrino, T.; Plank, C. Labelling of Cells with Quantum Dots. *Nanotechnology* **2005**, *16*, R9–R25.
5. Chan, W. C.; Maxwell, D. J.; Gao, X.; Bailey, R. E.; Han, M.; Nie, S. Luminescent Quantum Dots for Multiplexed Biological Detection and Imaging. *Curr. Opin. Biotechnol.* **2006**, *13*, 40–46.
6. Ballou, B.; Lagerholm, B. C.; Ernst, L. A.; Bruchez, M. P.; Waggoner, A. S. Noninvasive Imaging of Quantum Dots in Mice. *Bioconjugate Chem* **2004**, *15*, 79–86.
7. Gao, X.; Cui, Y.; Levenson, R. M.; Chung, L. W.; Nie, S. In Vivo Cancer Targeting and Imaging with Semiconductor Quantum Dots. *Nat. Biotechnol.* **2004**, *22*, 969–976.
8. Wu, X.; Liu, H.; Liu, J.; Haley, K. N.; Treadway, J. A.; Larson, J. P.; Ge, N.; Peale, F.; Bruchez, M. P. Immunofluorescent Labeling of Cancer Marker Her2 and Other Cellular Targets with Semiconductor Quantum Dots. *Nat. Biotechnol.* **2003**, *21*, 41–46.
9. Kalyuzhny, G.; Murray, R. W. Ligand Effects on Optical Properties of CdSe Nanocrystals. *J. Phys. Chem. B* **2005**, *109*, 7012–7021.
10. Kuno, M.; Lee, J. K.; Dabbousi, B. O.; Mikulec, F. V.; Bawendi, M. G. The Band Edge Luminescence of Surface Modified CdSe Nanocrystallites: Probing the Luminescing State. *J. Chem. Phys.* **1997**, *106*, 9869–9882.
11. Mekis, I.; Talapin, D. V.; Kornowski, A.; Haase, M.; Weller, H. One-Pot Synthesis of Highly Luminescent CdSe/CdS Core-Shell Nanocrystals via Organometallic and "Greener" Chemical Approaches. *J. Phys. Chem. B* **2003**, *107*, 7454–7462.
12. Torchilin, V. P. Recent Advances with Liposomes as Pharmaceutical Carriers. *Nat. Rev. Drug Discov.* **2005**, *4*, 145–160.
13. Derfus, A. M.; Chan, W. C.; Bhatia, S. N. Intracellular Delivery of Quantum Dots for Live Cell Labeling and Organelle Tracking. *Adv. Mater.* **2004**, *16*, 961–966.
14. Voura, E. B.; Jaiswal, J. K.; Mattoussi, H.; Simon, S. M. Tracking Metastatic Tumor Cell Extravasation with Quantum Dot Nanocrystals and Fluorescence Emission-Scanning Microscopy. *Nat. Med.* **2004**, *10*, 993–998.
15. Bullen, C.; Mulvaney, P. The Effects of Chemisorption on the Luminescence of CdSe Quantum Dots. *Langmuir* **2006**, *22*, 3007–3013.
16. Komoto, A.; Maenosono, S.; Yamaguchi, Y. Oscillating Fluorescence in an Unstable Colloidal Dispersion of CdSe/ZnS Core/Shell Quantum Dots. *Langmuir* **2004**, *20*, 8916–8923.
17. Gaunt, J. A.; Knight, A. E.; Windsor, S. A.; Chechik, V. Stability and Quantum Yield Effects of Small Molecule Additives on Solutions of Semiconductor Nanoparticles. *J. Colloid Interface Sci.* **2005**, *290*, 437–443.
18. van Sark, W. G. J. H.; Frederix, P. L. T. M.; Bol, A. A.; Gerritsen, H. C.; Meijerink, A. Blueing, Bleaching, and Blinking of Single CdSe/ZnS Quantum Dots. *ChemPhysChem* **2002**, *3*, 871–879.
19. Gregoriadis, G.; Davis, C. Stability of Liposomes in Vivo and in Vitro Is Promoted by Their Cholesterol Content and the Presence of Blood Cells. *Biochem. Biophys. Res. Commun.* **1979**, *89*, 1287–1293.
20. Kirby, C.; Clarke, J.; Gregoriadis, G. Cholesterol Content of Small Unilamellar Liposomes Controls Phospholipid Loss to High Density Lipoproteins in the Presence of Serum. *FEBS Lett.* **1980**, *111*, 324–328.
21. Kostarelos, K.; Emfietzoglou, D.; Papakostas, A.; Yang, W. H.; Ballangrud, A.; Sgouros, G. Binding and Interstitial Penetration of Liposomes within Avascular Tumor Spheroids. *Int. J. Cancer* **2004**, *112*, 713–721.
22. Smith, A. M.; Ruan, G.; Rhyner, M. N.; Nie, S. Engineering Luminescent Quantum Dots for in Vivo Molecular and Cellular Imaging. *Ann. Biomed. Eng.* **2006**, *34*, 3–14.
23. Alivisatos, A. P.; Gu, W.; Larabell, C. Quantum Dots as Cellular Probes. *Annu. Rev. Biomed. Eng* **2005**, *7*, 55–76.
24. Gao, X.; Yang, L.; Petros, J. A.; Marshall, F. F.; Simons, J. W.; Nie, S. In Vivo Molecular and Cellular Imaging with Quantum Dots. *Curr. Opin. Biotechnol.* **2005**, *16*, 63–72.
25. Pellegrino, T.; Manna, L.; Kudera, S.; Liedl, T.; Koktysh, D.; Rogach, A. L.; Keller, S.; Radler, J.; Natile, G.; Parak, W. J. Hydrophobic Nanocrystals Coated with an Amphiphilic Polymer Shell: A General Route to Water Soluble Nanocrystals. *Nano Lett.* **2004**, *4*, 703–707.
26. Mulder, W. J.; Koole, R.; Brandwijk, R. J.; Storm, G.; Chin, P. T.; Strijkers, G. J.; de Mello Donega, C.; Nicolay, K.; Griffioen, A. W. Quantum Dots with a Paramagnetic Coating as a Bimodal Molecular Imaging Probe. *Nano Lett.* **2006**, *6*, 1–6.
27. Dubertret, B.; Skourides, P.; Norris, D. J.; Noireaux, V.; Brivanlou, A. H.; Libchaber, A. In Vivo Imaging of Quantum Dots Encapsulated in Phospholipid Micelles. *Science* **2002**, *298*, 1759–1762.
28. Stroh, M.; Zimmer, J. P.; Duda, D. G.; Levchenko, T. S.; Cohen, K. S.; Brown, E. B.; Scadden, D. T.; Torchilin, V. P.; Bawendi, M. G.; Fukumura, D. Quantum Dots Spectrally Distinguish Multiple Species within the Tumor Milieu in Vivo. *Nat. Med.* **2005**, *11*, 678–682.
29. Chan, C. P.; Bruemmel, Y.; Seydack, M.; Sin, K. K.; Wong, L. W.; Merisko-Liversidge, E.; Trau, D.; Renneberg, R. Nanocrystal Biolabels with Releasable Fluorophores for Immunoassays. *Anal. Chem.* **2004**, *76*, 3638–3645.
30. Gopalakrishnan, G.; Danelon, C.; Izewska, P.; Prummer, M.; Bolinger, P. Y.; Geissbuhler, I.; Demurtas, D.; Dubochet, J.; Vogel, H. Multifunctional Lipid/Quantum Dot Hybrid Nanocontainers for Controlled Targeting of Live Cells. *Angew. Chem., Int. Ed.* **2006**, *45*, 5478–5483.
31. Hsieh, S. C.; Wang, F. F.; Lin, C. S.; Chen, Y. J.; Hung, S. C.; Wang, Y. J. The Inhibition of Osteogenesis with Human Bone Marrow Mesenchymal Stem Cells by CdSe/ZnS Quantum Dot Labels. *Biomaterials* **2006**, *27*, 1656–1664.
32. Ma, J.; Chen, Y. J.; Guo, J.; Wang, C. C.; Yang, W. L.; Xu, L.; Wang, P. N. Photostability of Thiol-Capped CdTe Quantum Dots in Living Cells: The Effect of Photo-Oxidation. *Nanotechnology* **2006**, *17*, 2083–2089.
33. Liu, S.; Lee, C. M.; Wang, S.; Lu, D. R. A New Bioimaging Carrier for Fluorescent Quantum Dots: Phospholipid Nanoemulsion Mimicking Natural Lipoprotein Core. *Drug Deliv.* **2006**, *13*, 159–164.
34. Jaiswal, J. K.; Mattoussi, H.; Mauro, J. M.; Simon, S. M. Long-Term Multiple Color Imaging of Live Cells Using Quantum Dot Bioconjugates. *Nat. Biotechnol.* **2003**, *21*, 47–51.
35. Silver, J.; Ou, W. Photoactivation of Quantum Dot Fluorescence Following Endocytosis. *Nano Lett.* **2005**, *5*, 1445–1449.
36. Courty, S.; Luccardini, C.; Bellaiche, Y.; Cappello, G.; Dahan, M. Tracking Individual Kinesin Motors in Living Cells Using Single Quantum-Dot Imaging. *Nano Lett.* **2006**, *6*, 1491–1495.
37. Srinivasan, C.; Lee, J.; Papadimitrakopoulos, F.; Silbart, L. K.; Zhao, M.; Burgess, D. J. Labeling and Intracellular Tracking of Functionally Active Plasmid DNA with Semiconductor Quantum Dots. *Mol. Ther.* **2006**, *14*, 192–201.
38. Chen, A. A.; Derfus, A. M.; Khetani, S. R.; Bhatia, S. N. Quantum Dots To Monitor RNAi Delivery and Improve Gene Silencing. *Nucleic Acids Res.* **2005**, *33*, e190 .
39. Krag, D.; Weaver, D.; Ashikaga, T.; Moffat, F.; Klimberg, V. S.; Shriver, C.; Feldman, S.; Kusminsky, R.; Gadd, M.; Kuhn, J. The Sentinel Node in Breast Cancer—A Multicenter Validation Study. *N. Engl. J. Med.* **1998**, *339*, 941–946.
40. Rubio, I. T.; Korourian, S.; Cowan, C.; Krag, D. N.; Colvert, M.; Klimberg, V. S. Sentinel Lymph Node Biopsy for Staging Breast Cancer. *Am. J. Surg.* **1998**, *176*, 532–537.
41. Harrington, K. J.; Rowlinson-Busza, G.; Syrigos, K. N.; Uster, P. S.; Vile, R. G.; Stewart, J. S. Pegylated Liposomes Have Potential as Vehicles for Intratumoral and Subcutaneous Drug Delivery. *Clin. Cancer Res.* **2000**, *6*, 2528–2537.

42. Nomura, T.; Nakajima, S.; Kawabata, K.; Yamashita, F.; Takakura, Y.; Hashida, M. Intratumoral Pharmacokinetics and in Vivo Gene Expression of Naked Plasmid DNA and Its Cationic Liposome Complexes after Direct Gene Transfer. *Cancer Res.* **1997**, *57*, 2681–2686.
43. Nomura, T.; Koreeda, N.; Yamashita, F.; Takakura, Y.; Hashida, M. Effect of Particle Size and Charge on the Disposition of Lipid Carriers after Intratumoral Injection into Tissue-Isolated Tumors. *Pharm. Res.* **1998**, *15*, 128–132.
44. Nomura, T.; Saikawa, A.; Morita, S.; Sakaeda Kakutani, T.; Yamashita, F.; Honda, K.; Takakura, Y.; Hashida, M. Pharmacokinetic Characteristics and Therapeutic Effects of Mitomycin C-Dextran Conjugates after Intratumoural Injection. *J. Controlled Release* **1998**, *52*, 239–252.
45. Bao, A.; Phillips, W. T.; Goins, B.; Zheng, X.; Sabour, S.; Natarajan, M.; Ross Woolley, F.; Zavaleta, C.; Otto, R. A. Potential Use of Drug Carried-Liposomes for Cancer Therapy via Direct Intratumoral Injection. *Int. J. Pharm.* **2006**, *316*, 162–169.
46. Moschetta, A.; Frederik, P. M.; Portincasa, P.; vanBerge-Henegouwen, G. P.; van Erpecum, K. J. Incorporation of Cholesterol in Sphingomyelin-Phosphatidylcholine Vesicles Has Profound Effects on Detergent-Induced Phase Transitions. *J. Lipid Res.* **2002**, *43*, 1046–1053.